iScience

CellPress
OPEN ACCESS

Article

Metabolic and functional remodeling of colonic macrophages in response to high-fat diet-induced obesity

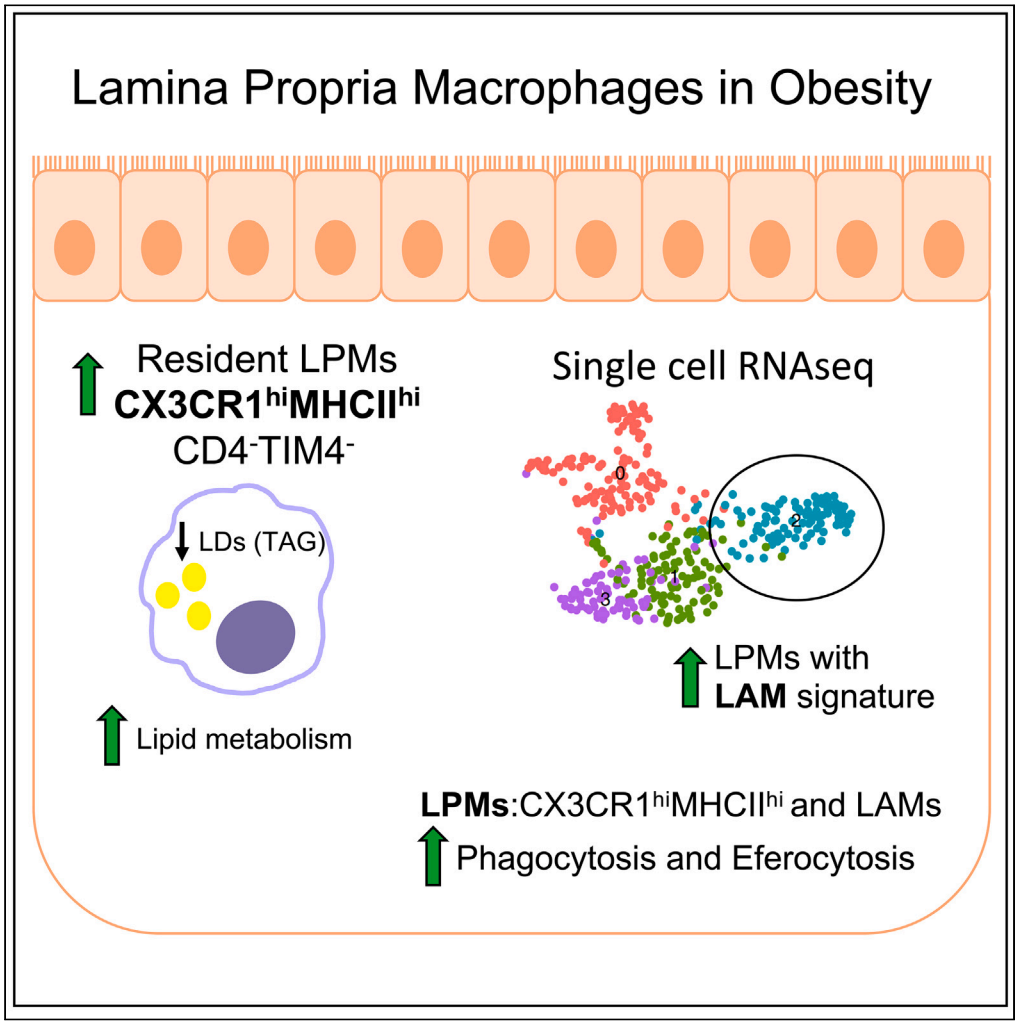

Angela Castoldi, David E. Sanin, Nikki van Teijlingen Bakker, ..., Erika L. Pearce, Edward J. Pearce, Niels Olsen Saraiva Camara

niels@icb.usp.br

Highlights

CX3CR1^{hi}MHCII^{hi}CD4^{-} TIM4^{-} LPMs are increased in obesity

CX3CR1^{hi}MHCII^{hi} LPMs have decreased neutral lipids accumulation and TG content

Lipid-associated macrophages (LAMs) are increased in obese lamina propria

LPMs from obese mice display increased phagocytosis and efferocytosis

Castoldi et al., iScience *26*, 107719
October 20, 2023
https://doi.org/10.1016/j.isci.2023.107719

iScience

CellPress
OPEN ACCESS

Article

Metabolic and functional remodeling of colonic macrophages in response to high-fat diet-induced obesity

Angela Castoldi,[1,2,3] David E. Sanin,[2,4] Nikki van Teijlingen Bakker,[2] Cristhiane F. Aguiar,[1] Lauar de Brito Monteiro,[2] Nisha Rana,[2] Katarzyna M. Grzes,[2,4] Agnieszka M. Kabat,[2,4] Jonathan Curtis,[2,4] Alanna M. Cameron,[2] George Caputa,[2] Tiago Antônio de Souza,[1] Fabrício O. Souto,[3] Joerg M. Buescher,[5] Joy Edwards-Hicks,[2] Erika L. Pearce,[2,4] Edward J. Pearce,[2,4,6] and Niels Olsen Saraiva Camara[1,6,7,*]

SUMMARY

Little is known about the effects of high-fat diet (HFD)-induced obesity on resident colonic lamina propria (LP) macrophages (LPMs) function and metabolism. Here, we report that obesity and diabetes resulted in increased macrophage infiltration in the colon. These macrophages exhibited the residency phenotype CX3CR1^{hi}MHCII^{hi} and were CD4^{-}TIM4^{-}. During HFD, resident colonic LPM exhibited a lipid metabolism gene expression signature that overlapped that used to define lipid-associated macrophages (LAMs). Via single-cell RNA sequencing, we identified a sub-cluster of macrophages, increased in HFD, that were responsible for the LAM signature. Compared to other macrophages in the colon, these cells were characterized by elevated glycolysis, phagocytosis, and efferocytosis signatures. CX3CR1^{hi}MHCII^{hi} colonic resident LPMs had fewer lipid droplets (LDs) and decreased triacylglycerol (TG) content compared to equivalent cells in lean mice and exhibited increased phagocytic capacity, suggesting that HFD induces adaptive responses in LPMs to limit bacterial translocation.

INTRODUCTION

The low-grade inflammatory response in obesity initially results from excessive nutrient accumulation that culminates in altered metabolic homeostasis. Sustained subsequent systemic inflammation involves changes in gut microbiota and increased gut permeability, which are associated with the maintenance of immune cell activation status, and associated comorbidities seen in obese individuals.[1–5]

Intestinal inflammation in obese subjects and in mice is subtle compared to that seen in adipose tissue. In obesity, there are broadly more infiltrating immune cells within the lamina propria (LP).[6] This is consistent with the fact that obesity triggers innate immune responses with increased interleukin (IL)-1β and adaptive immune response with increased T helper 1 (Th1) and Th17 cells in both the small and large intestine.[6–11] Despite the fact that there are changes in the immune cell compartment of the intestine during obesity, it remains unclear whether resident macrophages within this tissue play a role in the inflammatory state. In the majority of tissues, resident macrophages are derived from embryonic precursors that populate the tissue before birth and maintain themselves by self-renewal in the tissue during adulthood, with only minor contributions from blood monocytes. The intestine is an exception to this rule since the macrophage population (MHCII^{hi}CX3CR1^{hi}) in this organ requires constant replenishment by blood monocytes throughout adulthood.[12] A small pool of self-maintaining CD4^{+}TIM4^{+} macrophages was reported to exist in the adult intestine in mice; these persist independent of replenishment by blood monocytes.[13,14] Another population of CD4^{+}TIM4^{-} macrophages with a slow turnover from blood monocytes and a CD4^{-}TIM4^{-} population completely dependent on blood monocyte replenishment can also be found in mouse LP.[13] As monocytes enter the LP, they undergo a differentiation process whereby they first express major histocompatibility complex II (MHCII), followed by F4/80, CD64, and CX3CR1.[15,16] Intestinal resident macrophages have a role in maintenance of tissue homeostasis, inflammation, and inducing resolution after inflammation.[16] During colitis, the terminal differentiation of monocytes into mature resident macrophages (MHCII^{hi}CX3CR1^{hi}) is disrupted,[16] and evidence suggests a causal link between defects in resolution of intestinal inflammation and altered monocyte-macrophage differentiation, with the accumulation of cells that are

[1]Department of Immunology, University of Sao Paulo, Sao Paulo, Brazil
[2]Department of Immunometabolism, Max Planck Institute of Immunobiology and Epigenetics, Freiburg im Breisgau, Germany
[3]Institute Keizo Asami, Federal University of Pernambuco, Pernambuco, Brazil
[4]Bloomberg-Kimmel Institute for Cancer Immunotherapy, Department of Oncology, Johns Hopkins University School of Medicine, Baltimore, MD 21287, USA
[5]Metabolomics Facility, Max Planck Institute of Epigenetics and Immunobiology, Freiburg im Breisgau, Germany
[6]These authors contributed equally
[7]Lead contact
*Correspondence: niels@icb.usp.br
https://doi.org/10.1016/j.isci.2023.107719

considered to be immature macrophages causing impaired bacterial clearance and excessive cytokine secretion in patients with inflammatory bowel disease (IBD).[17,18]

Colonic macrophages have been found to play an important role in the induction of insulin resistance under high-fat diet (HFD). CCR2 expression and inflammation were found to be increased in the colon after 12 weeks of HFD feeding, corroborating increased monocyte recruitment to this site, and blocking monocyte, and thereby macrophage recruitment into the colon improved metabolic parameters.[19] However, the role of the other populations of macrophages in the colon during HFD has not been explored. Lipid-associated macrophages (LAMs), a subset of macrophages defined by a distinct lipid metabolism-associated signature, have recently been described to play a role in regulating gains in adiposity during obesity.[20] LAMs are increased in adipose tissue during obesity and recognized to arise from circulating monocytes. They characteristically express Trem2, a sensor of extracellular lipids which is involved in phagocytosis, lipid catabolism, and energy metabolism. LAMs were found to benefit systemic metabolism, preventing adipocyte hypertrophy, systemic hypercholesterolemia, inflammation, and glucose intolerance. Since the original description, LAMs have been described in several additional disease states, including non-alcoholic steatohepatitis (NASH), where they were found in aggregates in hepatic crown-like structures and were associated with protection against liver fibrosis.[21] In atherosclerosis, LAMs are thought to contribute to the calcification of atherosclerotic lesions.[22] Moreover, LAMs appear to be associated with the pathogenesis of Alzheimer disease.[23] In breast cancer, LAMs were distributed near adipocytes and characterized by an M2-like activation signature and were noted to be highly phagocytic, and their depletion was associated with protective anti-tumor effects.[24] Despite this growing realization that LAMs are present in a variety of diseases and associated with, depending on context, both positive and negative outcomes, these cells have not been studied in the LP.

In the present study, we report that obesity increases macrophage infiltration in the colon and that in this setting macrophages acquire the residency CX3CR1^{hi}MHCII^{hi} phenotype. Furthermore, we show that the CX3CR1^{hi}MHCII^{hi} macrophages that populate the colon in obesity are mainly CD4^{-}TIM4^{-}. We found that during HFD, CX3CR1^{hi}MHCII^{hi} colonic resident LP macrophages (LPMs) display an increased lipid metabolism signature. Additionally, we found that the CX3CR1^{hi}MHCII^{hi} colonic resident LPMs have decreased lipid droplet (LD) accumulation and decreased triacylglycerol (TG) content, which is associated with increased fatty acid oxidation (FAO). CX3CR1^{hi}MHCII^{hi} colonic resident LPMs showed increased phagocytic capacity in HFD-fed mice, suggesting that increased lipid metabolism is an adaptive response of these cells to limit bacterial translocation and maintenance of gut homeostasis. Further, through single-cell RNA sequencing (scRNA-seq), we identified a cluster of macrophages expressing genes consistent with the LAM signature, including genes associated with increased phagocytosis and efferocytosis. Our data indicate that LAMs develop within the LP during HFD.

RESULTS

HFD feeding increases colonic resident CX3CR1^{hi} macrophages infiltration

We investigated whether HFD-induced obesity affects colonic LPMs. We used CX3CR1$^{+/gfp}$ mice fed normal chow (lean) or HFD (60% fat) for 12 weeks. Compared to lean mice, HFD-fed mice gained a significant amount of fat mass (Figure S1A) and had increased glucose intolerance, decreased insulin sensitivity (Figure S1B), increased serum LPS (lipopolysaccharides) (Figure S1C), decreased occludin protein expression in the large intestine (Figure S1D), and shorter colons (Figure S1E). The total number and frequency of CD64^{+}CD11b^{+} colonic LP macrophages were increased because of HFD (Figures 1A–1C). The majority of cells in the broad CD64^{+}CD11b^{+} population were CX3CR1^{hi}MHCII^{hi} LPMs (Figures 1D–1F). This suggests that the majority of newly infiltrating macrophages acquire the expression of residency markers.

Long-lived CD4^{+}TIM4^{+} resident LPMs are decreased upon HFD

Recently, a population of long-lived macrophages expressing CD4 and TIM4 was shown to populate the intestinal LP.[13] The frequency of this population was comparable to the frequency of the blood monocyte-dependent populations in adult mice.[13] We found that HFD feeding resulted in a decrease in the frequency of CX3CR1^{hi}MHCII^{hi}CD4^{+}TIM4^{+} population from the colonic LP (Figures 1G and 1H). There was also a decrease in CX3CR1^{hi}MHCII^{hi}CD4^{+}TIM4^{-} cells (Figures 1G and 1I). The resident macrophages that populate the colonic LP on HFD are mainly CX3CR1^{hi}MHCII^{hi} CD4^{-}TIM4^{-} (Figures 1G and 1J). Together, our data show that HFD increases CX3CR1^{hi}MHCII^{hi} LPMs in the colon; moreover, the frequency of long-lived CD4^{+}TIM4^{+} macrophages is decreased and CD4^{-} TIM4^{-} macrophages become the dominant population in mice fed HFD.

Colonic CX3CR1^{hi} MHCII^{hi} LPMs display a lipid-associated phenotype and increased activation state

We sorted CX3CR1^{hi}MHCII^{hi} LPMs from lean and HFD-fed mice at the end of HFD feeding and used RNA sequencing (RNA-seq) to ask whether HFD leads to changes in gene expression. We found that 167 genes were regulated by > one (1) fold change (Figure S2A). Among these differentially expressed genes (DEGs), 40 were up-regulated and 127 genes were down-regulated (Figure S2A). Further analysis was restricted to the most significantly ($p \leq 0.01$) differentially regulated genes (Figure 2A). Genes in this category indicate that HFD promotes changes in the expression of genes that are engaged in inflammation, such as *Tlr2*,[25] *Vcam1*,[26] and the negative regulator of IL-1 signaling, *Il1r2*,[27] and genes related to lipid metabolism, such as *Lpl*,[28] which is also a gene in the FA biosynthetic pathway, *Abcg1*,[29] *Ppargc1a*,[30] and *Aqp9*[31] (Figures 2A–2F). The lipid metabolism-associated genes are among genes expressed by LAMs,[20] suggesting that HFD induces the LPMs to resemble LAMs.

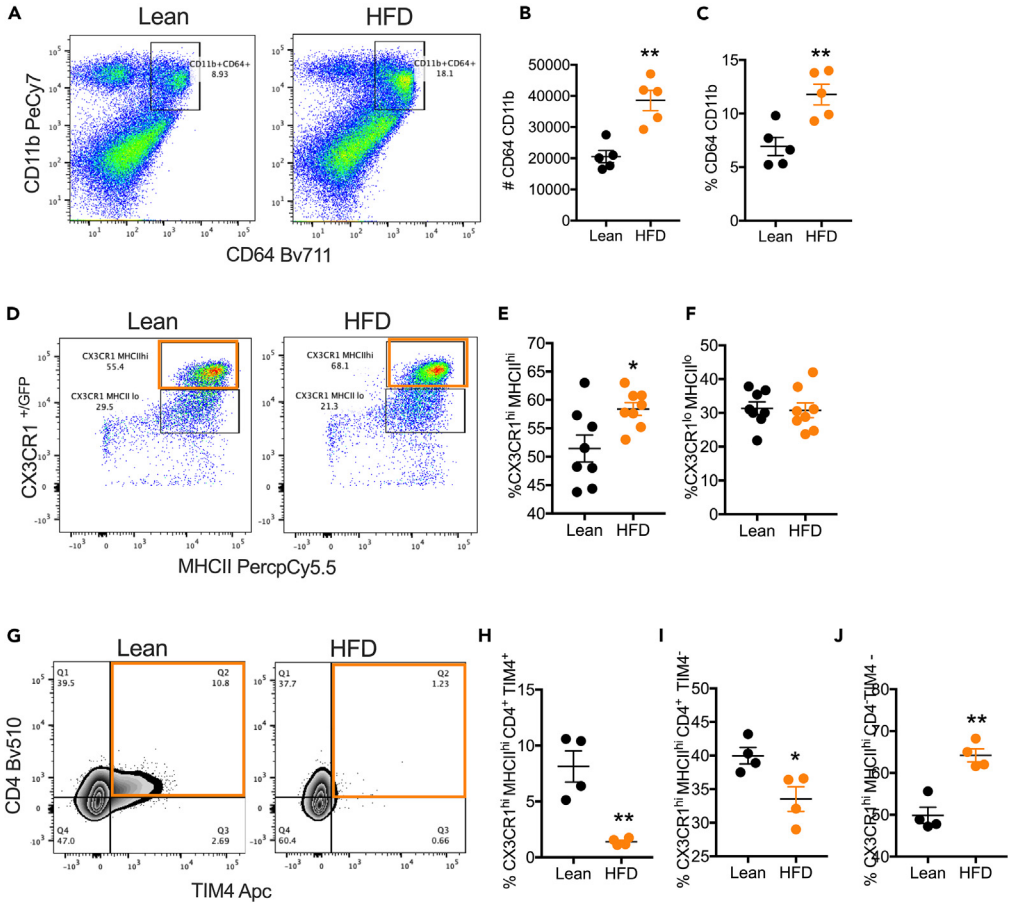

Figure 1. HFD increases macrophage infiltration in the colonic lamina propria

(A–C) Analysis by flow cytometry of global macrophages (CD64 CD11b) in the LP of lean and HFD-fed mice. Showing the total number (B) and the percentage (C) (n = 5 mice per group).

(D–F) Analysis of MHCII CX3CR1 macrophages showing increased MHCII^{hi}CX3CR1^{hi} (E) and no difference in CX3CR1^{lo}MHCII^{lo} (F) (n = 8 mice per group).

(G) Flow cytometry analysis of long-lived CD4 TIM4 LPMs gated on CX3CR1^{hi}MHCII^{hi} LPMs.

(H) Percentage of long-lived CD4^{+}TIM4^{+} LPMs.

(I) Percentage of long-lived CD4^{+}TIM4^{-} LPMs.

(J) Percentage of long-lived CD4^{-} TIM4^{-} LPMs (n = 4 mice per group). (Data presented as mean ± SEM. p values calculated with unpaired two-tailed Student's *t* test. *p < 0.05; **p < 0.01.).

Enrichment analysis based on hypergeometric distribution followed by false discovery rate (FDR) correction for Gene Ontology (GO) terms using the 14 up-regulated genes ($p \leq 0.01$) showed enriched biological processes related to lipid metabolism (Figure 2G). Heatmaps of LAM-associated gene[20] expression showed regulation in HFD-fed compared to lean mice (Figure 2H).

Moreover, the *RNA-seq* data provided support the flow cytometry-based finding that HFD leads to a decrease in LP CD4^{+}TIM4^{+} macrophages (Figure 1G), revealing decreased *Timd4* expression in LPMs sorted from HFD-fed mice, while the expression of *Cd4* and the macrophage markers *Cx3cr1*, *Fcgr1*, and *Lyz2* was not affected (Figures S2B–S2G).

In parallel, we took a targeted approach using gene expression and flow cytometry to measure the effects of HFD on the expression of known markers of macrophage activation. While expression of *Cd86, Cd80,* and *Mrc1* by colonic CX3CR1^{hi}MHCII^{hi} LPMs was unaffected (Figures 3A–3C), the surface expression of the proteins that these genes encode, CD86, CD80, and CD206, was increased by HFD-feeding mice (Figures 3D–3J). A similar pattern was observed for CX3CR1^{lo}MHCII^{lo} LPMs (Figure S3).

Single-cell profile of colonic LP macrophages after HFD feeding

We used scRNA-seq of sorted CD45^{+} colonic LP cells to analyze HFD-induced immune changes in the colon. LP cells were isolated from a total of 6 mice (3 HFD and 3 lean) and loaded onto the 10X Genomics Chromium platform. After sequencing, aggregation of the samples, quality control, removal of contaminating CD45^{-} cells, and exclusion of cells resembling doublets, a total of 8,207 cells remained (4,613 cells from lean, 3,594 cells from HFD). Seventeen transcriptionally distinct clusters of cells were identified by generating a Uniform Manifold

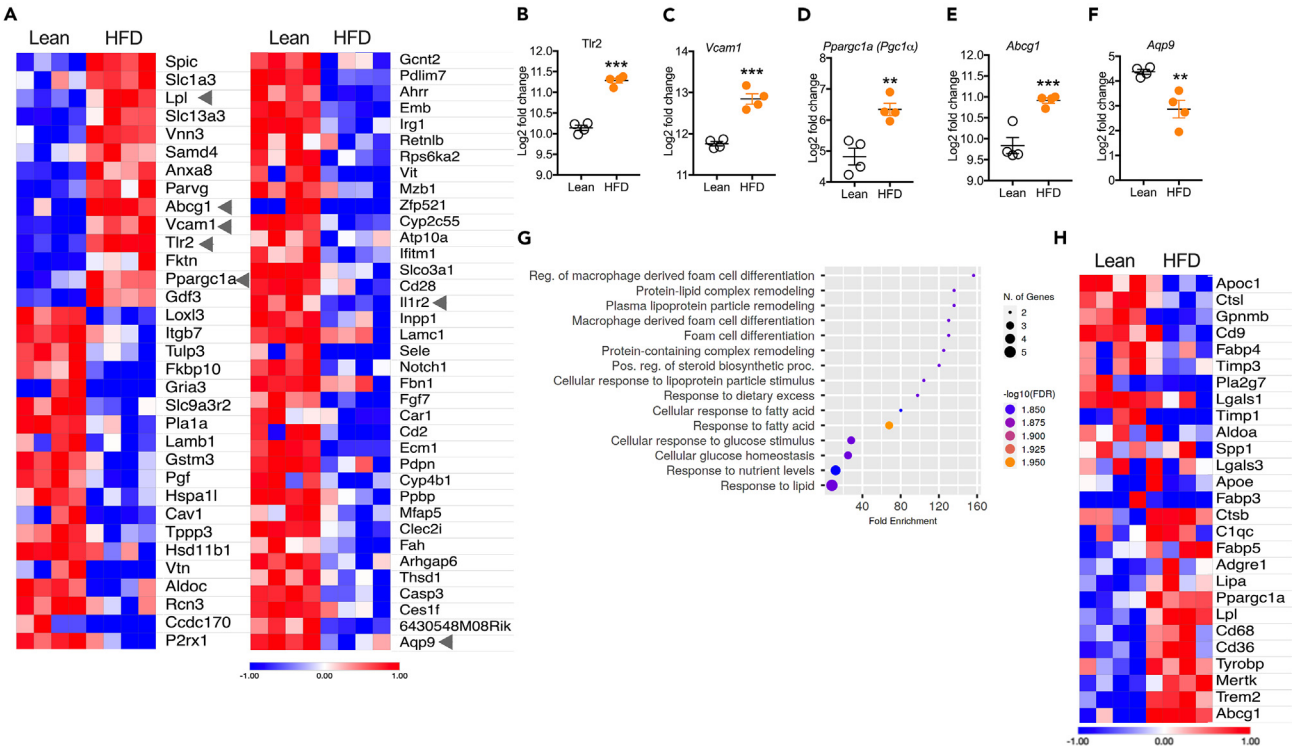

Figure 2. HFD modulates gene expression in the colonic CX3CR1^{hi}MHCII^{hi} LPMs

(A) RNA sequencing analysis of the most significantly regulated genes ($p < 0.01$) in CX3CR1^{hi}MHCII^{hi} LPMs from lean and HFD-fed mice.

(B–F) Comparison of (B) *Tlr2*, (C)*Vcam1*, (D) *Ppargc1a*, (E) *Abcg1*, (F) *Aqp9* Log2 Fold change between lean and HFD (n = 4 mice per group).

(G) Fold Enrichment analysis of top15 biological processes related to the up-regulated ($p < 0.01$) genes in CX3CR1^{hi}MHCII^{hi} LPMs from HFD-fed mice.

(H) Heatmap of Lipid metabolism-related genes in CX3CR1^{hi}MHCII^{hi} LPMs from lean and HFD-fed mice (n = 4 mice per group). (Data presented as mean ± SEM. p values calculated with unpaired two-tailed Student's *t* test. **$p < 0.01$; ***$p < 0.001$.).

Approximation and Projection (UMAP) from the transcriptome data using principal-component analysis (Figure S4A). Within these clusters, we identified distinct cell types based on the DEGs (Figures S4A and S4B). We did not detect different clusters between HFD and lean conditions (Figure S4B).

Using an unbiased cell classification based on scGate annotation,[32] we identified clusters with Lymphoid cell signature, T cell signature, CD4$^+$ T cell signature, T regulatory cell signature, CD8$^+$ T cell signature, B cell signature, Natural killer (NK) cell signature, Myeloid cell signature, and Macrophage signature (Figure S4C). The cluster classified by scGate annotation as Macrophages was further shown to express the macrophage-defining genes *Lyz2, Cx3cr1, Fcgr1, Cd68,* and *Adgre1*, indicating that cluster 5 is likely macrophages (Figure S4D). To examine changes in this population, we re-clustered cells within cluster 5 into a new UMAP, in which four clusters were identifiable (Figures 4A and 4B). At this resolution, differences in proportion between HFD and lean conditions were evident, with cluster 0 smaller and cluster 2 larger in HFD (Figure 4C). In order to understand the differences between these clusters, we next calculated gene expression scores using the UCell[33] metric to analyze the function of these cells (Figure 4D). Cluster 2, which is expanded in HFD-fed mice, had a decreased heat shock signature, strong interferon response and glycolysis signatures, and no difference, compared to other clusters, in the overall OXPHOS signature. Corroborating the bulk RNA-seq data indicating increased lipid metabolism in resident colonic CX3CR1^{hi}MHCII^{hi} LPMs (Figures 2A–2H), we found a significantly higher LAM signature (Figure 4D). Moreover, an increased efferocytosis signature was also detected in cluster 2 (Figure 4D). Based on significantly different gene expression ($p < 0.01$) in cluster 2, we applied enrichment analysis based on hypergeometric distribution followed by FDR correction for GO terms (Figure 4E). The 10 top regulated biological processes in cells in cluster 2 included phagocytosis, inflammatory/immune response, and defense response (Figure 4E). *Trem2,* a specific LAM marker, was expressed mainly by cluster 2 in the colonic LPMs (Figure S4E). This suggests that HFD leads to an increase of an LP population of macrophages that resembles LAMs with an activated phenotype, associated with increased glycolysis, phagocytosis, and efferocytosis.

The neutral lipid content of colonic resident macrophages is reduced during HFD

Our data indicate that HFD induces changes in the expression of genes linked to lipid metabolism in colonic LPMs. To explore this further, we analyzed the lipid content of colonic CX3CR1^{hi}MHCII^{hi} LPMs. Using Bodipy staining, we observed a decrease in neutral lipids/LDs in cells from HFD mice (Figure 5A). Consistent with this, lipidomics indicated that compared to cells from lean conditions, colonic CX3CR1^{hi}MHCII^{hi} LPMs

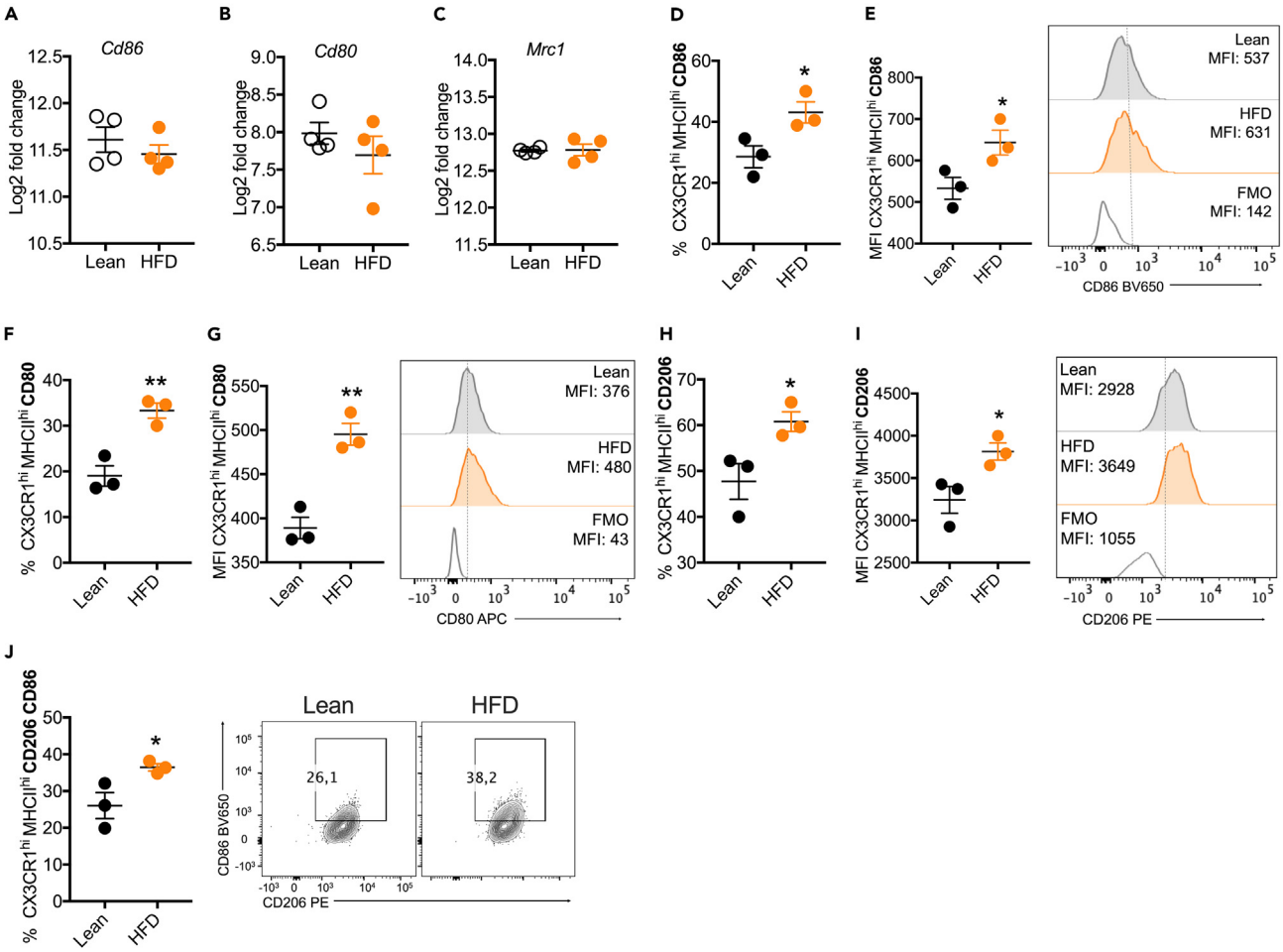

Figure 3. HFD modulates CD86, CD80, and CD206 in CX3CR1^{hi}MHCII^{hi} LPMs

(A–C) Log2 Fold change of gene expression from the RNA sequencing of *Cd86*, *Cd80*, and *Mrc1* by CX3CR1^{hi}MHCII^{hi} LPMs between lean and HFD (n = 4 mice per group).

(D and E) Percentage of CX3CR1^{hi}MHCII^{hi} LPMs expressing CD86 and (E) MFI of CD86.

(F and G) Percentage of CX3CR1^{hi}MHCII^{hi} LPMs expressing CD80 and (G) MFI of CD80.

(H and I) Percentage of CX3CR1^{hi}MHCII^{hi} LPMs expressing CD206 and (I) MFI of CD206.

(J) Percentage of CX3CR1^{hi}MHCII^{hi} LPMs expressing CD206 and CD86 (n = 3 mice per group). (Data presented as mean ± SEM. p values calculated with unpaired two-tailed Student's *t* test. *p < 0.05; **p < 0.01.).

from HFD mice have lower levels of stored TGs (Figure 5B), especially TG-48, TG-50, and TG-52 (Figures S5A and S5B), and no changes in cholesteryl esters (CEs) (Figure 5C), although the total lipid content of these cells tended to be higher (Figure 5D) together with the stores of hexosylceramides (HexCer) 24-0, 22-0, 24-1, and 16-0 (Figures S5A and S5C). We reasoned that the increased total lipid may be accounted for by increased expression of *Cd36* (Figure 2H), a major mediator of cellular fatty acid uptake.[34] Further, we reasoned that the observed decrease in TG content in colonic CX3CR1^{hi}MHCII^{hi}LPMs from HFD mice might be explained by increased FAO coupled to TG hydrolysis. Consistent with this, CPT1a expression measured by flow cytometry was increased in the LP macrophages from mice on HFD (Figure 5E). The increased FAO might be due to an increase in mitochondrial mass measured by Mito Tracker Deep Red FM which stains active mitochondria (Figure 5F).

HFD feeding increases colonic resident macrophage phagocytic capacity

A major recognized function of resident colonic LPMs for maintenance of tissue homeostasis is phagocytosis.[15] Indeed, we found that phagocytosis and efferocytosis signatures were enriched in cluster 2 (Figure 4D). We asked whether we could measure this function of LPMs to conclude that it was affected by HFD feeding. We found that colonic CX3CR1^{hi}MHCII^{hi} LPMs from HFD-fed mice had increased phagocytic capacity compared to the equivalent cells from lean mice (Figures 6A and 6B). This was associated with increased reactive oxygen species (ROS) (Figure 6C), which corroborates increased phagocytosis.[35] Overall, our findings indicate that during HFD feeding a population of CX3CR1^{hi}MHCII^{hi} macrophages develops in the LP that resembles LAMs. This population exhibits enhanced phagocytic capacity.

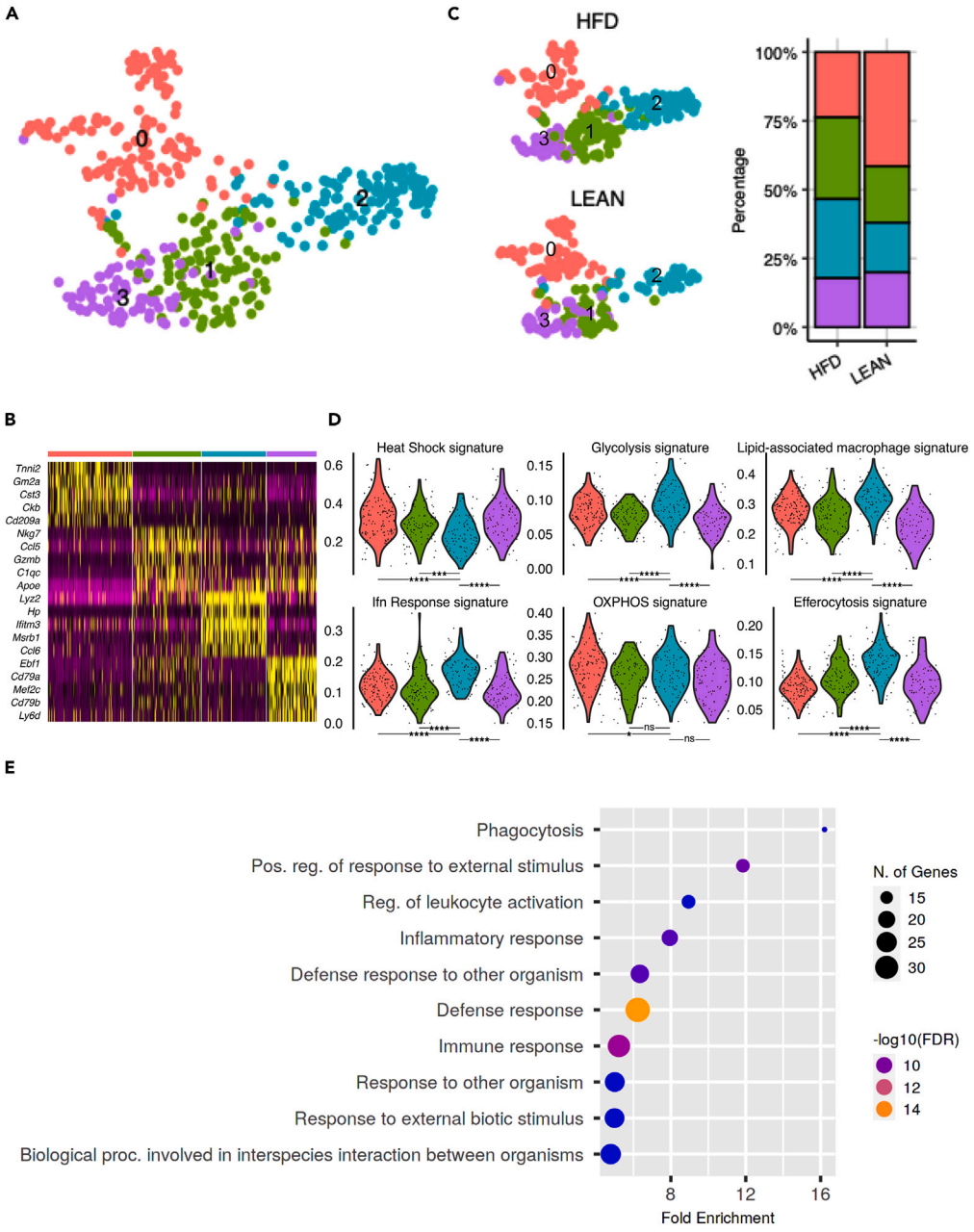

Figure 4. HFD increases the proportion of colonic macrophages with an LAM signature

(A and B) Single-cell RNA sequencing of CD45^{+} cells from the LP isolated from 6 mice (3 (12W) HFD and 3 lean) and loaded onto the 10X Genomics Chromium platform. Macrophage Cluster (Cluster 5) was identified according to the expression of *Lyz2*, *Cx3cr1*, *Fcgr1*, *Cd68*, and *Adgre1* and re-clustered in a new UMAP divided in 4 clusters.

(C) Percentage of each cluster in lean and HFD condition.

(D and E) Gene expression scores calculated using the R package UCell (E) Enrichment analysis of top10 biological processes related to the up-regulated ($p < 0.01$) genes in cluster 2. (Data presented as mean ± SEM. p values calculated with one-way ANOVA. *$p < 0.05$; ***$p < 0.001$; ****$p < 0.0001$.).

DISCUSSION

We have found that HFD increases the percentage and total number of CD64^{+}CD11b^{+} macrophages in the intestine and that a component of this response comprises an increase in CX3CR1^{hi}MHCII^{hi} colonic resident LPMs. We speculate that this reflects increased replenishment by blood monocytes which would be appropriate for the intestinal immune system, where constant exposure to bacteria and other materials requires rapid and aggressive responses to potential pathogens to maintain homeostasis, especially in obesity where gut

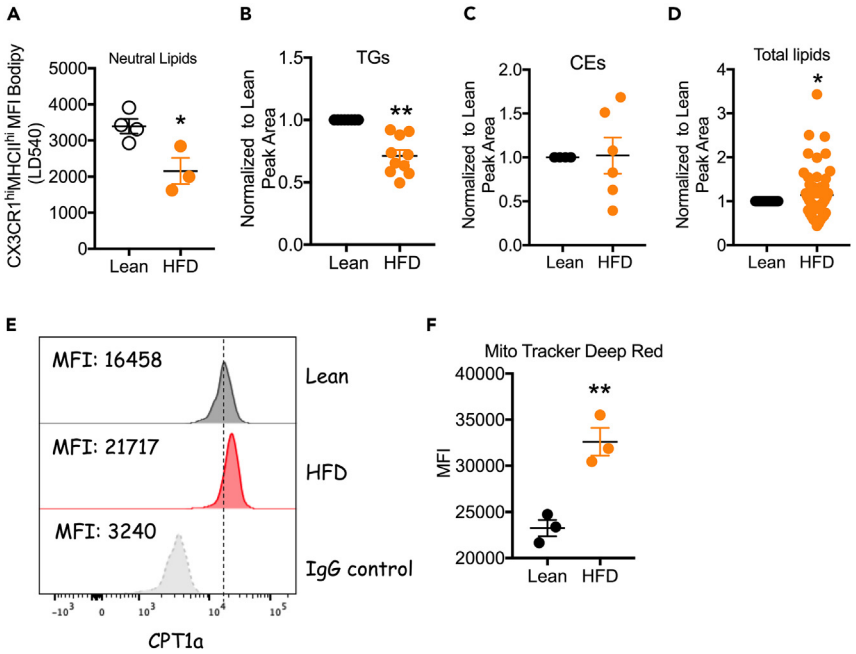

Figure 5. CX3CR1^{hi}MHCII^{hi} LPMs from HFD-fed mice show decreased neutral lipids accumulation and increased fatty acid oxidation

(A) neutral lipid accumulation in CX3CR1^{hi}MHCII^{hi} LPMs detected using LD540 staining (n = 3–4 mice per group).

(B) Total triacylglycerol (TG) in 50.000 sorted CX3CR1^{hi}MHCII^{hi} LPMs analyzed by lipidomics. Each dot represents the average of each TG specie detected by lipidomics in three samples of each condition.

(C) Total Cholesteryl Esters (CEs) in 50.000 sorted CX3CR1^{hi}MHCII^{hi} LPMs analyzed by lipidomics. Each dot represents the average of each CE specie detected by lipidomics in three samples of each condition (n = 3 mice per group).

(D) Total lipid content in 50.000 sorted CX3CR1^{hi}MHCII^{hi} LPMs analyzed by lipidomics. Each dot represents the average of each lipid specie detected by lipidomics in three samples of each condition (n = 3 mice per group).

(E) Flow cytometry analysis of CPT1a expression in CX3CR1^{hi}MHCII^{hi} LPMs (n = pool of 3 mice per group).

(F) Mitochondrial mass measured by Mito Tracker Deep Red in lean and HFD CX3CR1^{hi}MHCII^{hi} (MFI, median fluorescence intensity) (n = 3 mice per group). (Data presented as mean ± SEM. p values calculated with unpaired two-tailed Student's *t* test. *p < 0.05; **p < 0.01.).

permeability is increased. It is not surprising that we do not see a decrease in the CX3CR1^{hi}MHCII^{hi} population since the low-grade inflammation induced in obesity by HFD is chronic and systemic and does not disrupt the processes that normally induce the full differentiation of resident macrophages.[15,16] Intestinal resident macrophages have a role in maintenance of tissue homeostasis, inflammation, and resolution after inflammation. During intestinal inflammation, the terminal differentiation of monocytes into mature resident macrophages (CX3CR1^{hi}) is disrupted.[16] We found that HFD is not sufficient to disrupt differentiation but rather promoted increased differentiation toward the MHCII^{hi}CX3CR1^{hi} phenotype. It is unclear whether this reflects loss of intrinsic factors that usually specify full maturation, or if chronic low-grade inflammation actively revises these processes. We postulate that these might be associated with the chronic low-grade inflammation induced by HFD and increased lipid metabolism and are an adaptation that prevents inflammatory bowel disease development in this setting.

Previous studies have found that innate gut immunity is involved in metabolic disease as mice fed an HFD have elevated levels of Toll-like receptor (TLR) 4, tumor necrosis factor (TNF), and nuclear factor κB (NF-κB) in the gut[36,37] and increased proinflammatory colonic macrophage infiltration.[19] This agrees with our idea of increased infiltration and differentiation of blood monocytes into resident macrophages. In obese humans, an increase in the number of leukocytes in the intestinal mucosa and a change toward proinflammatory macrophages have been found and these proinflammatory macrophages are potentially recruited via blood monocytes.[6,9,38] Our data indicate that the inflammation induced by HFD requires recruitment of blood monocytes to differentiate into CX3CR1^{hi}MHCII^{hi} macrophages.

We found that HFD increases protein expression of CD86 and CD206 by CX3CR1^{hi}MHCII^{hi} macrophages; however, no significant changes were observed at mRNA levels. We speculate that the protein levels are more conserved than mRNA levels of these genes. The increased CD86 expression suggests increased co-stimulation of T cells by these resident macrophages,[39] and the expression of CD206 indicates that these cells present a mature phenotype and suggests an anti-inflammatory phenotype, in agreement with the role of resident macrophages, highly phagocytic without inducing local inflammation.[14,40] This suggests that upon HFD, CX3CR1^{hi}MHCII^{hi} LPMs maintain their anti-inflammatory profile in order to keep intestinal homeostasis. Consistent with this, our scRNA-seq shows that HFD results in an increased proportion of a cluster of highly phagocytic related macrophages (Cluster 2). Rohm et al.[38] found, in the human intestine, five populations of macrophages: three monocyte-derived proinflammatory populations able to secrete proinflammatory cytokines,[16,18,41] and two

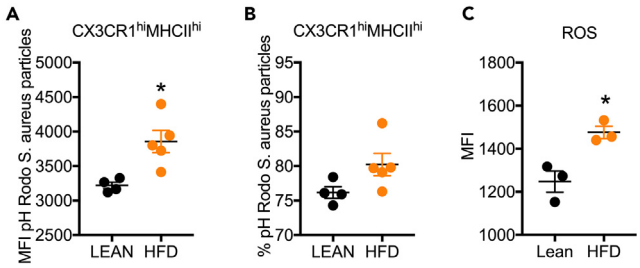

Figure 6. CX3CR1^{hi}MHCII^{hi} LPMs from HFD-fed mice have increased phagocytic capacity

(A and B) Phagocytosis assay using pH Rodo S. aureus particles in CX3CR1^{hi}MHCII^{hi} LPMs from lean and HFD-fed mice (MFI) and (B) percentage (n = 4–5 mice per group).

(C) Cellular ROS measured *ex vivo* in CX3CR1^{hi}MHCII^{hi} LPMs from lean and HFD-fed mice (n = 3 mice per group). (Data presented as mean ± SEM. p values calculated with unpaired two-tailed Student's *t* test. *p < 0.05.).

resident/mature (anti-inflammatory) macrophages populations. The inflammatory population was increased in all sections of the intestine of obese individuals. Furthermore, increased proinflammatory macrophages in the gut of mice fed an HFD were reported previously,[38] and colon-specific macrophage depletion improved glucose tolerance and insulin sensitivity.[38] However, our single-cell data are a more robust characterization of heterogeneous macrophage populations in the gut.

scRNA-seq allowed us to define a macrophage population with increased phagocytosis/efferocytosis and lipid metabolism. Functionally, LAMs were characterized by a canonical functional signature of lipid metabolism, enhanced phagocytosis, and elements of M2 activation,[20,24] which is also observed in our model. LAMs were first described as necessary for controlling metabolic homeostasis.[20] Depletion of these cells caused increased adipocyte hypertrophy, systemic hypercholesterolemia, inflammation, and glucose intolerance in mice.[20] Moreover, LAMs were also found to be induced by local lipid exposure in steatotic regions of the murine and human liver.[42] In agreement, in NASH, TIM4^{+} Kupfer cells (KCs) decrease and TIM4^{-} monocyte-derived macrophages are increased in the liver. This monocyte-derived macrophage population consists of cells expressing *Cx3cr1/Ccr2* and cells expressing LAM markers which were associated with crown-like structures and appear to protect the liver against adverse remodeling during NASH, preventing liver fibrosis.[21]

We also found that under HFD, long-lived resident LPMs that express CD4 and TIM4 are decreased from the colonic LP, as well as decreased gene expression of *Timd4*. These cells correspond to a small fraction of self-maintaining macrophages that are independent of blood monocytes.[13,14] HFD seems to accelerate the decrease of these cells from the intestine, something that normally occurs as mice age.[13] In addition, lipotoxicity would also impact their survival since HFD confers a lipid-rich environment, especially in adipose tissue macrophages[43]; however, we did not observe accumulation of LDs in CX3CR1^{hi}MHCII^{hi} LPMs. Moreover, we found increased proportion of CD4^{-}TIM4^{-} macrophages in colonic LP in obese mice. Elsewhere, the CD4^{-}TIM4^{-} macrophage population in the colonic LP was reported to be completely dependent on blood monocyte replenishment.[13] The increased resident LPM infiltration upon HFD might be related to an intrinsic mechanism to maintain their survival to support phagocytosis.

The LAM-associated signature found in the phagocytic macrophage cluster, which is increased in HFD-fed mice, may be necessary for homeostasis of the gut during obesity. This seems to be associated with balancing lipid accumulation. Consistently, we found decreased LD accumulation in CX3CR1^{hi}MHCII^{hi} LPMs from HFD-fed mice. This reflected decreased TG accumulation and increased expression of genes related to FAO and lipolysis, which was also associated with increased CPT1a protein expression by these cells, and increased mitochondrial mass measured by Mito Tracker Deep Red, indicating increased mitochondrial activity supporting the idea that there is increased fat catabolism in these cells. Inflammatory macrophages were shown to accumulate LD because they are not able to oxidize lipids and this accumulation is necessary for proinflammatory cytokine release.[44] We also found increased HexCer species, which is in accordance with our and others' previous studies showing increased accumulation in activated macrophages, PMNs, and CD4^{+} T cells.[44,45] More studies are needed to understand the role of HexCer in macrophages.

However, efficient phagocytosis was also shown to require fatty acids hydrolysis[46] and LPMs are known to be highly phagocytic,[14] patrolling the gut to maintain homeostasis. Moreover, we detected increased ROS in CX3CR1^{hi}MHCII^{hi} LPMs, consistent with increased phagocytosis.

Corroborating, we found an increased efferocytosis signature in the macrophage cluster that was increased in HFD LP. It was previously shown that efferocytosis of apoptotic cells by macrophages anchor the resolution of intestinal inflammation, preventing necrosis and further inflammation, and programming macrophages for tissue repair.[47,48] Moreover, efferocytosis by intestinal macrophages is dependent on COX2,[47] which is necessary for prostaglandins synthesis.[49] Prostaglandin synthesis is necessary for phagocytosis in inflammatory macrophages,[44] supporting the role of lipid metabolism and LAMs in contributing to homeostasis in the gut during HFD. In addition, we postulate that the increased phagocytosis might reflect the increased prevalence of cluster 2 macrophages in mice fed HFD.

Our study provides a new perspective on the phenotype of resident LPMs upon HFD feeding and obesity. We conclude that HFD induces changes in the populations profile of colonic resident LPMs, increasing activation, depleting long-lived CD4^{+}TIM4^{+} LPMs, and increasing monocyte-derived LAMs displaying increased phagocytosis capacity in order to maintain gut homeostasis during HFD feeding.

Limitations of the study

Our study showed that obesity and diabetes induced changes in resident LPMs lipid metabolism impacting on their phagocytic capacity. However, we were not able to show that if blocking FA oxidation in LPMs would increase LDs accumulation and consequently decrease phagocytosis by these cells leading to a higher bacterial translocation. Yet, the role of LP LAMs, showed to be increased in obesity, was also not further explored and we do not show if depleting LAMs from the LP would increase the risk of obesity and diabetes.

QUANTIFICATION AND STATISTICAL ANALYSIS

Statistical analysis was performed using Prism 7 software (Graphpad) or R (for the gene expression scores) and results are represented as mean ± SEM. Comparisons for two groups were calculated using unpaired two-tailed Student's *t* test, comparisons of more than two groups were calculated using one-way ANOVA multiple comparison test. We observed normal distribution and no difference in variance between groups in individual comparisons. Statistical significance: *$p < 0.05$; **$p < 0.01$; ***$p < 0.001$; ****$p < 0.0001$. Further details on statistical analysis are listed in the figure legends.

STAR★METHODS

Detailed methods are provided in the online version of this paper and include the following:

- KEY RESOURCES TABLE
- RESOURCE AVAILABILITY
  - Lead contact
  - Materials availability'
  - Data and code availability
- EXPERIMENTAL MODEL AND STUDY PARTICIPANTS DETAILS
- METHOD DETAILS
  - Metabolic parameters analysis
  - Determination of serum LPS
  - Wester blotting
  - Lamina propria cells/macrophages isolation
  - Flow cytometry
  - RNA sequencing
  - Single cell barcoding and library preparation
  - Lipidomics

SUPPLEMENTAL INFORMATION

Supplemental information can be found online at https://doi.org/10.1016/j.isci.2023.107719.

ACKNOWLEDGMENTS

We thank the members of the Pearce laboratories, the FACS, and Deep Sequencing facilities at the Max Planck Institute of Immunobiology and Epigenetics, the members of Camara's Laboratory, and CEFAP-USP for technical support. A.C. was supported by the CAPES/Alexander von Humboldt Fellowship Foundation (88881.136065/2017-01) and FAPESP grants 2015/18121-4, 2017/05264-7, and 2017/00721-0. This study was also financed in part by CAPES, finance code 001.

AUTHOR CONTRIBUTIONS

A.C, E.J.P., and N.O.S.C. conceptualized the study, designed the research, and interpreted the data. D.E.S, T.A.S., and N.R. analyzed bioinformatics data. A.C., J.E-H., and J.B. analyzed Lipidomics data. A.C., N.v.T.B., C.F.A., L.B.M., N.R., K.M.G., A.M.K., J.C., A.M.C., G.C., T.A.S., and F.O.S. performed experiments. E.L.P. helped with project insights. N.O.S.C., E.L.P., and E.J.P. acquired funding. A.C., E.J.P., and N.O.S.C. wrote the manuscript.

DECLARATION OF INTERESTS

E.J.P. and E.L.P. declare that they are Founders of Rheos Medicines. E.L.P. is a member of the Scientific Advisory Board of Immunomet Therapeutics.

INCLUSION AND DIVERSITY

We support inclusive, diverse, and equitable conduct of research.

Received: January 19, 2023
Revised: July 17, 2023
Accepted: August 22, 2023
Published: August 25, 2023

REFERENCES

1. Gregor, M.F., and Hotamisligil, G.S. (2011). Inflammatory mechanisms in obesity. Annu. Rev. Immunol. *29*, 415–445. https://doi.org/10.1146/annurev-immunol-031210-101322.
2. Sell, H., Habich, C., and Eckel, J. (2012). Adaptive immunity in obesity and insulin resistance. Nat. Rev. Endocrinol. *8*, 709–716. https://doi.org/10.1038/nrendo.2012.114.
3. Kratz, M., Coats, B.R., Hisert, K.B., Hagman, D., Mutskov, V., Peris, E., Schoenfelt, K.Q., Kuzma, J.N., Larson, I., Billing, P.S., et al. (2014). Metabolic dysfunction drives a mechanistically distinct proinflammatory phenotype in adipose tissue macrophages. Cell Metab. *20*, 614–625. https://doi.org/10.1016/j.cmet.2014.08.010.
4. Rosen, E.D., and Spiegelman, B.M. (2014). What we talk about when we talk about fat. Cell *156*, 20–44. https://doi.org/10.1016/j.cell.2013.12.012.
5. Chawla, A., Nguyen, K.D., and Goh, Y.P.S. (2011). Macrophage-mediated inflammation in metabolic disease. Nat. Rev. Immunol. *11*, 738–749. https://doi.org/10.1038/nri3071.
6. Monteiro-Sepulveda, M., Touch, S., Mendes-Sá, C., André, S., Poitou, C., Allatif, O., Cotillard, A., Fohrer-Ting, H., Hubert, E.L., Remark, R., et al. (2015). Jejunal T Cell Inflammation in Human Obesity Correlates with Decreased Enterocyte Insulin Signaling. Cell Metab. *22*, 113–124. https://doi.org/10.1016/j.cmet.2015.05.020.
7. Veilleux, A., Mayeur, S., Bérubé, J.C., Beaulieu, J.F., Tremblay, E., Hould, F.S., Bossé, Y., Richard, D., and Levy, E. (2015). Altered intestinal functions and increased local inflammation in insulin-resistant obese subjects: a gene-expression profile analysis. BMC Gastroenterol. *15*, 119. https://doi.org/10.1186/s12876-015-0342-y.
8. Martins, L.M.S., Perez, M.M., Pereira, C.A., Costa, F.R.C., Dias, M.S., Tostes, R.C., Ramos, S.G., de Zoete, M.R., Ryffel, B., Silva, J.S., and Carlos, D. (2018). Interleukin-23 promotes intestinal T helper type17 immunity and ameliorates obesity-associated metabolic syndrome in a murine high-fat diet model. Immunology *154*, 624–636. https://doi.org/10.1111/imm.12946.
9. Luck, H., Tsai, S., Chung, J., Clemente-Casares, X., Ghazarian, M., Revelo, X.S., Lei, H., Luk, C.T., Shi, S.Y., Surendra, A., et al. (2015). Regulation of obesity-related insulin resistance with gut anti-inflammatory agents. Cell Metab. *21*, 527–542. https://doi.org/10.1016/j.cmet.2015.03.001.
10. Winer, D.A., Luck, H., Tsai, S., and Winer, S. (2016). The Intestinal Immune System in Obesity and Insulin Resistance. Cell Metab. *23*, 413–426. https://doi.org/10.1016/j.cmet.2016.01.003.
11. Hong, C.P., Park, A., Yang, B.G., Yun, C.H., Kwak, M.J., Lee, G.W., Kim, J.H., Jang, M.S., Lee, E.J., Jeun, E.J., et al. (2017). Gut-Specific Delivery of T-Helper 17 Cells Reduces Obesity and Insulin Resistance in Mice. Gastroenterology *152*, 1998–2010. https://doi.org/10.1053/j.gastro.2017.02.016.
12. Ginhoux, F., and Guilliams, M. (2016). Tissue-Resident Macrophage Ontogeny and Homeostasis. Immunity *44*, 439–449. https://doi.org/10.1016/j.immuni.2016.02.024.
13. Shaw, T.N., Houston, S.A., Wemyss, K., Bridgeman, H.M., Barbera, T.A., Zangerle-Murray, T., Strangward, P., Ridley, A.J.L., Wang, P., Tamoutounour, S., et al. (2018). Tissue-resident macrophages in the intestine are long lived and defined by Tim-4 and CD4 expression. J. Exp. Med. *215*, 1507–1518. https://doi.org/10.1084/jem.20180019.
14. De Schepper, S., Verheijden, S., Aguilera-Lizarraga, J., Viola, M.F., Boesmans, W., Stakenborg, N., Voytyuk, I., Schmidt, I., Boeckx, B., Dierckx de Casterlé, I., et al. (2018). Self-Maintaining Gut Macrophages Are Essential for Intestinal Homeostasis. Cell *175*, 400–415.e13. https://doi.org/10.1016/j.cell.2018.07.048.
15. Bain, C.C., Bravo-Blas, A., Scott, C.L., Perdiguero, E.G., Geissmann, F., Henri, S., Malissen, B., Osborne, L.C., Artis, D., and Mowat, A.M. (2014). Constant replenishment from circulating monocytes maintains the macrophage pool in the intestine of adult mice. Nat. Immunol. *15*, 929–937. https://doi.org/10.1038/ni.2967.
16. Bain, C.C., Scott, C.L., Uronen-Hansson, H., Gudjonsson, S., Jansson, O., Grip, O., Guilliams, M., Malissen, B., Agace, W.W., and Mowat, A.M. (2013). Resident and pro-inflammatory macrophages in the colon represent alternative context-dependent fates of the same Ly6Chi monocyte precursors. Mucosal Immunol. *6*, 498–510. https://doi.org/10.1038/mi.2012.89.
17. Smith, A.M., Rahman, F.Z., Hayee, B., Graham, S.J., Marks, D.J.B., Sewell, G.W., Palmer, C.D., Wilde, J., Foxwell, B.M.J., Gloger, I.S., et al. (2009). Disordered macrophage cytokine secretion underlies impaired acute inflammation and bacterial clearance in Crohn's disease. J. Exp. Med. *206*, 1883–1897. https://doi.org/10.1084/jem.20091233.
18. Bernardo, D., Marin, A.C., Fernández-Tomé, S., Montalban-Arques, A., Carrasco, A., Tristán, E., Ortega-Moreno, L., Mora-Gutiérrez, I., Díaz-Guerra, A., Caminero-Fernández, R., et al. (2018). Human intestinal pro-inflammatory CD11c. Mucosal Immunol. *11*, 1114–1126. https://doi.org/10.1038/s41385-018-0030-7.
19. Kawano, Y., Nakae, J., Watanabe, N., Kikuchi, T., Tateya, S., Tamori, Y., Kaneko, M., Abe, T., Onodera, M., and Itoh, H. (2016). Colonic Pro-inflammatory Macrophages Cause Insulin Resistance in an Intestinal Ccl2/Ccr2-Dependent Manner. Cell Metab. *24*, 295–310. https://doi.org/10.1016/j.cmet.2016.07.009.
20. Jaitin, D.A., Adlung, L., Thaiss, C.A., Weiner, A., Li, B., Descamps, H., Lundgren, P., Bleriot, C., Liu, Z., Deczkowska, A., et al. (2019). Lipid-Associated Macrophages Control Metabolic Homeostasis in a Trem2-Dependent Manner. Cell *178*, 686–698.e14. https://doi.org/10.1016/j.cell.2019.05.054.
21. Daemen, S., Gainullina, A., Kalugotla, G., He, L., Chan, M.M., Beals, J.W., Liss, K.H., Klein, S., Feldstein, A.E., Finck, B.N., et al. (2021). Dynamic Shifts in the Composition of Resident and Recruited Macrophages Influence Tissue Remodeling in NASH. Cell Rep. *34*, 108626. https://doi.org/10.1016/j.celrep.2020.108626.
22. Cochain, C., Vafadarnejad, E., Arampatzi, P., Pelisek, J., Winkels, H., Ley, K., Wolf, D., Saliba, A.E., and Zernecke, A. (2018). Single-Cell RNA-Seq Reveals the Transcriptional Landscape and Heterogeneity of Aortic Macrophages in Murine Atherosclerosis. Circ. Res. *122*, 1661–1674. https://doi.org/10.1161/CIRCRESAHA.117.312509.
23. Andreone, B.J., Przybyla, L., Llapashtica, C., Rana, A., Davis, S.S., van Lengerich, B., Lin, K., Shi, J., Mei, Y., Astarita, G., et al. (2020). Alzheimer's-associated PLCγ2 is a signaling node required for both TREM2 function and the inflammatory response in human microglia. Nat. Neurosci. *23*, 927–938. https://doi.org/10.1038/s41593-020-0650-6.
24. Liu, Z., Gao, Z., Li, B., Li, J., Ou, Y., Yu, X., Zhang, Z., Liu, S., Fu, X., Jin, H., et al. (2022). Lipid-associated macrophages in the tumor-adipose microenvironment facilitate breast cancer progression. Oncoimmunology *11*, 2085432. https://doi.org/10.1080/2162402X.2022.2085432.
25. Himes, R.W., and Smith, C.W. (2010). Tlr2 is critical for diet-induced metabolic syndrome in a murine model. FASEB J. *24*, 731–739. https://doi.org/10.1096/fj.09-141929.
26. Chung, K.J., Chatzigeorgiou, A., Economopoulou, M., Garcia-Martin, R., Alexaki, V.I., Mitroulis, I., Nati, M., Gebler, J., Ziemssen, T., Goelz, S.E., et al. (2017). A self-sustained loop of inflammation-driven inhibition of beige adipogenesis in obesity. Nat. Immunol. *18*, 654–664. https://doi.org/10.1038/ni.3728.
27. Shimizu, K., Nakajima, A., Sudo, K., Liu, Y., Mizoroki, A., Ikarashi, T., Horai, R., Kakuta, S., Watanabe, T., and Iwakura, Y. (2015). IL-1 receptor type 2 suppresses collagen-induced arthritis by inhibiting IL-1 signal on macrophages. J. Immunol. *194*, 3156–3168. https://doi.org/10.4049/jimmunol.1402155.
28. Chang, H.R., Josefs, T., Scerbo, D., Gumaste, N., Hu, Y., Huggins, L.A., Barrett, T.J., Chiang, S.S., Grossman, J., Bagdasarov, S., et al. (2019). Role of LpL (Lipoprotein Lipase) in Macrophage Polarization In Vitro and In Vivo. Arterioscler. Thromb. Vasc. Biol. *39*, 1967–1985. https://doi.org/10.1161/ATVBAHA.119.312389.
29. Out, R., Hoekstra, M., Hildebrand, R.B., Kruit, J.K., Meurs, I., Li, Z., Kuipers, F., Van Berkel, T.J.C., and Van Eck, M. (2006). Macrophage ABCG1 deletion disrupts lipid homeostasis in alveolar macrophages and moderately influences atherosclerotic lesion development in LDL receptor-deficient mice. Arterioscler. Thromb. Vasc. Biol. *26*, 2295–2300. https://doi.org/10.1161/01.ATV.0000237629.29842.4c.

30. McCarthy, C., Lieggi, N.T., Barry, D., Mooney, D., de Gaetano, M., James, W.G., McClelland, S., Barry, M.C., Escoubet-Lozach, L., Li, A.C., et al. (2013). Macrophage PPAR gamma Co-activator-1 alpha participates in repressing foam cell formation and atherosclerosis in response to conjugated linoleic acid. EMBO Mol. Med. *5*, 1443–1457. https://doi.org/10.1002/emmm.201302587.
31. Cui, G., Staron, M.M., Gray, S.M., Ho, P.C., Amezquita, R.A., Wu, J., and Kaech, S.M. (2015). IL-7-Induced Glycerol Transport and TAG Synthesis Promotes Memory CD8+ T Cell Longevity. Cell *161*, 750–761. https://doi.org/10.1016/j.cell.2015.03.021.
32. Andreatta, M., Berenstein, A.J., and Carmona, S.J. (2022). scGate: marker-based purification of cell types from heterogeneous single-cell RNA-seq datasets. Bioinformatics *38*, 2642–2644. https://doi.org/10.1093/bioinformatics/btac141.
33. Andreatta, M., and Carmona, S.J. (2021). UCell: Robust and scalable single-cell gene signature scoring. Comput. Struct. Biotechnol. J. *19*, 3796–3798. https://doi.org/10.1016/j.csbj.2021.06.043.
34. Chen, Y., Zhang, J., Cui, W., and Silverstein, R.L. (2022). CD36, a signaling receptor and fatty acid transporter that regulates immune cell metabolism and fate. J. Exp. Med. *219*, e20211314. https://doi.org/10.1084/jem.20211314.
35. Wang, P., Geng, J., Gao, J., Zhao, H., Li, J., Shi, Y., Yang, B., Xiao, C., Linghu, Y., Sun, X., et al. (2019). Macrophage achieves self-protection against oxidative stress-induced ageing through the Mst-Nrf2 axis. Nat. Commun. *10*, 755. https://doi.org/10.1038/s41467-019-08680-6.
36. de La Serre, C.B., Ellis, C.L., Lee, J., Hartman, A.L., Rutledge, J.C., and Raybould, H.E. (2010). Propensity to high-fat diet-induced obesity in rats is associated with changes in the gut microbiota and gut inflammation. Am. J. Physiol. Gastrointest. Liver Physiol. *299*, G440–G448. https://doi.org/10.1152/ajpgi.00098.2010.
37. Ding, S., Chi, M.M., Scull, B.P., Rigby, R., Schwerbrock, N.M.J., Magness, S., Jobin, C., and Lund, P.K. (2010). High-fat diet: bacteria interactions promote intestinal inflammation which precedes and correlates with obesity and insulin resistance in mouse. PLoS One *5*, e12191. https://doi.org/10.1371/journal.pone.0012191.
38. Rohm, T.V., Fuchs, R., Müller, R.L., Keller, L., Baumann, Z., Bosch, A.J.T., Schneider, R., Labes, D., Langer, I., Pilz, J.B., et al. (2021). Obesity in Humans Is Characterized by Gut Inflammation as Shown by Pro-Inflammatory Intestinal Macrophage Accumulation. Front. Immunol. *12*, 668654. https://doi.org/10.3389/fimmu.2021.668654.
39. Muntjewerff, E.M., Meesters, L.D., and van den Bogaart, G. (2020). Antigen Cross-Presentation by Macrophages. Front. Immunol. *11*, 1276. https://doi.org/10.3389/fimmu.2020.01276.
40. Wright, P.B., McDonald, E., Bravo-Blas, A., Baer, H.M., Heawood, A., Bain, C.C., Mowat, A.M., Clay, S.L., Robertson, E.V., Morton, F., et al. (2021). The mannose receptor (CD206) identifies a population of colonic macrophages in health and inflammatory bowel disease. Sci. Rep. *11*, 19616. https://doi.org/10.1038/s41598-021-98611-7.
41. Thiesen, S., Janciauskiene, S., Uronen-Hansson, H., Agace, W., Högerkorp, C.M., Spee, P., Håkansson, K., and Grip, O. (2014). CD14(hi)HLA-DR(dim) macrophages, with a resemblance to classical blood monocytes, dominate inflamed mucosa in Crohn's disease. J. Leukoc. Biol. *95*, 531–541. https://doi.org/10.1189/jlb.0113021.
42. Guilliams, M., Bonnardel, J., Haest, B., Vanderborght, B., Wagner, C., Remmerie, A., Bujko, A., Martens, L., Thoné, T., Browaeys, R., et al. (2022). Spatial proteogenomics reveals distinct and evolutionarily conserved hepatic macrophage niches. Cell *185*, 379–396.e38. https://doi.org/10.1016/j.cell.2021.12.018.
43. Prieur, X., Mok, C.Y.L., Velagapudi, V.R., Núñez, V., Fuentes, L., Montaner, D., Ishikawa, K., Camacho, A., Barbarroja, N., O'Rahilly, S., et al. (2011). Differential lipid partitioning between adipocytes and tissue macrophages modulates macrophage lipotoxicity and M2/M1 polarization in obese mice. Diabetes *60*, 797–809. https://doi.org/10.2337/db10-0705.
44. Castoldi, A., Monteiro, L.B., van Teijlingen Bakker, N., Sanin, D.E., Rana, N., Corrado, M., Cameron, A.M., Hässler, F., Matsushita, M., Caputa, G., et al. (2020). Triacylglycerol synthesis enhances macrophage inflammatory function. Nat. Commun. *11*, 4107. https://doi.org/10.1038/s41467-020-17881-3.
45. Alarcon-Barrera, J.C., von Hegedus, J.H., Brouwers, H., Steenvoorden, E., Ioan-Facsinay, A., Mayboroda, O.A., Ondo-Mendez, A., and Giera, M. (2020). Lipid metabolism of leukocytes in the unstimulated and activated states. Anal. Bioanal. Chem. *412*, 2353–2363. https://doi.org/10.1007/s00216-020-02460-8.
46. Chandak, P.G., Radovic, B., Aflaki, E., Kolb, D., Buchebner, M., Fröhlich, E., Magnes, C., Sinner, F., Haemmerle, G., Zechner, R., et al. (2010). Efficient phagocytosis requires triacylglycerol hydrolysis by adipose triglyceride lipase. J. Biol. Chem. *285*, 20192–20201. https://doi.org/10.1074/jbc.M110.107854.
47. Meriwether, D., Jones, A.E., Ashby, J.W., Solorzano-Vargas, R.S., Dorreh, N., Noori, S., Grijalva, V., Ball, A.B., Semis, M., Divakaruni, A.S., et al. (2022). Macrophage COX2 Mediates Efferocytosis, Resolution Reprogramming, and Intestinal Epithelial Repair. Cell. Mol. Gastroenterol. Hepatol. *13*, 1095–1120. https://doi.org/10.1016/j.jcmgh.2022.01.002.
48. Bosurgi, L., Cao, Y.G., Cabeza-Cabrerizo, M., Tucci, A., Hughes, L.D., Kong, Y., Weinstein, J.S., Licona-Limon, P., Schmid, E.T., Pelorosso, F., et al. (2017). Macrophage function in tissue repair and remodeling requires IL-4 or IL-13 with apoptotic cells. Science *356*, 1072–1076. https://doi.org/10.1126/science.aai8132.
49. FitzGerald, G.A. (2003). COX-2 and beyond: Approaches to prostaglandin inhibition in human disease. Nat. Rev. Drug Discov. *2*, 879–890. https://doi.org/10.1038/nrd1225.
50. Love, M.I., Huber, W., and Anders, S. (2014). Moderated estimation of fold change and dispersion for RNA-seq data with DESeq2. Genome Biol. *15*, 550. https://doi.org/10.1186/s13059-014-0550-8.
51. Spandl, J., White, D.J., Peychl, J., and Thiele, C. (2009). Live cell multicolor imaging of lipid droplets with a new dye, LD540. Traffic *10*, 1579–1584. https://doi.org/10.1111/j.1600-0854.2009.00980.x.
52. Bhardwaj, V., Heyne, S., Sikora, K., Rabbani, L., Rauer, M., Kilpert, F., Richter, A.S., Ryan, D.P., and Manke, T. (2019). snakePipes: facilitating flexible, scalable and integrative epigenomic analysis. Bioinformatics *35*, 4757–4759. https://doi.org/10.1093/bioinformatics/btz436.
53. Ge, S.X., Jung, D., and Yao, R. (2020). ShinyGO: a graphical gene-set enrichment tool for animals and plants. Bioinformatics *36*, 2628–2629. https://doi.org/10.1093/bioinformatics/btz931.
54. Matyash, V., Liebisch, G., Kurzchalia, T.V., Shevchenko, A., and Schwudke, D. (2008). Lipid extraction by methyl-tert-butyl ether for high-throughput lipidomics. J. Lipid Res. *49*, 1137–1146. https://doi.org/10.1194/jlr.D700041-JLR200.

STAR★METHODS

KEY RESOURCES TABLE

REAGENT or RESOURCE	SOURCE	IDENTIFIER
Antibodies		
Anti-mouse CD16/32	BioLegend	Cat#101302; RRID: AB_312801
Live/Dead™ Near IR	ThermoFisher	Cat#L10119
Anti-mouse CD45	BioLegend	Cat#157211; RRID: AB_2876534
Anti-mouse CD11b	BioLegend	Cat#101216; RRID: AB_312799
Anti-mouse CD64	BioLegend	Cat#139311; RRID: AB_2563846
Anti-mouse MHCII	BioLegend	Cat#107626; RRID: AB_2191071
Anti-mouse TIM4	BioLegend	Cat#129906; RRID: AB_1227798
Anti-mouse CD4	BioLegend	Cat#100559; RRID: AB_2562608
Anti-mouse CD86	BioLegend	Cat#105036; RRID: AB_2686973
Anti-mouse CD80	BioLegend	Cat#104714; RRID: AB_313135
Anti-mouse CD206	BioLegend	Cat#141706; RRID: AB_10895754
CPT1a	Proteintech	Cat#15184-1-AP; RRID: AB_2084676
Anti-rabbit Alexa Fluor 647	ThermoFisher	Cat#A27040; RRID: AB_2536101
Anti-mouse Occludin	BD Biosciences	Cat#611090; RRID: AB_398403
Anti-mouse Beta actin	Cell Signaling	Cat#3700; RRID: AB_2242334
Anti-mouse	Cell Signaling	Cat#7076; RRID: AB_330924
Chemicals, peptides, and recombinant proteins		
Collagenase Type VIII	Sigma	Cat#C2139
FBS	Gibco	Lot. 1640960
RPMI 1640	ThermoFisher	Cat#21875158
HEPES	ThermoFisher	Cat#15630130
Percoll	Sigma	Cat#P1644
DNase I	Sigma	Cat#11284932001
Critical commercial assays		
pHrodo™ Red Staphylococcus aureus Bioparticles™	ThermoFisher	Cat#A10010
BODIPY LD 540	Developed by Prof. Christoph Tiele[51]	N/A
CellROX Deep Red	Invitrogen	Cat#C10491
Mito Tracker Deep Red	ThermoFisher	Cat#M22426
LAL kit- terminal QCL1000	LONZA	
RNAqueous-Micro Total RNA Isolation kit	Invitrogen	Cat#AM1391
TruSeq stranded mRNA kit	Illumina	N/A
Deposited data		
scRNAseq and RNAseq	GEO	GSE171330; GSE240228
Experimental models: Organisms/strains		
C57BL/6J mice	The Jackson Laboratory	JAX: 000664
CX3CR1 GFP mice	The Jackson Laboratory	JAX: 005582
Software and algorithms		
Prism 7	Graphpad	RRID: SCR_000306
ImageJ	https://imagej.nih.gov	RRID: SCR_003070
FlowJo v.10.1	Tree Star	RRID: SCR_008520

(*Continued on next page*)

Continued

REAGENT or RESOURCE	SOURCE	IDENTIFIER
R	Lucent Technologies	RRID: SCR_001905
Morpheus	Broad Institute	RRID: SCR_017386
Cell Ranger 2.2	10X Genomics	RRID: SCR_017344
ShinyGO 0.76	http://bioinformatics.sdstate.edu/go76/	RRID: SCR_019213
DESeq2	Love et al., 2014[50]	RRID: SCR_015687
Other		
Rodent Diet 60% kcal from fat	Research Diets, Inc	Cat#D12492

RESOURCE AVAILABILITY

Lead contact

Further information and requests for reagents and resources should be directed to and will be fulfilled by the lead contacts, Niels Olsen Saraiva Câmara (niels@icb.usp.com.br).

Materials availability'

This study did not generate new unique reagents.

Data and code availability

- Data: Single Cell RNA-sequence and RNA-sequence data have been deposited in Gene Expression Omnibus (GEO) under the primary accession code GSE171330 and GSE240228 respectively.
- Code: This paper does not report original code.
- Other items: No other new unique reagent was generated. Any additional information required to reanalyze the data reported in this paper is available from the lead contact upon request.

EXPERIMENTAL MODEL AND STUDY PARTICIPANTS DETAILS

Experiments were performed in C57BL/6 CX3CR1 GFP heterozygous male mice aged 4–6 weeks. The mice were maintained in specific pathogen-free conditions under protocols approved by the animal care committee of the Regierungspräsidium Freiburg, Germany, and University of São Paulo in compliance with all relevant ethical regulations. Obesity was induced by *ad libitum* feeding of C57BL/6 CX3CR1 GFP heterozygous male mice for 12 weeks with irradiated high fat diet (HFD) (Rodent Diet 60% kcal from fat). Control diet (chow) containing 24% protein, 47.5% carbohydrate, and 4.9% fat, was given to age and sex matched animals as a control group (Lean).

METHOD DETAILS

Metabolic parameters analysis

Peripheral response to glucose was assessed by glucose tolerance test (GTT). Glucose (2g/Kg body weight) was administered intraperitoneally in mice fasted for 12 h. Glucose levels in blood were determined before and after 15, 30, 60, 90 and 120 min from glucose administration. The insulin response (insulin tolerance test (ITT) was examined after fasting mice for 6 h. Blood glucose levels were determined before and after 15, 30, 60, 90 and 120 min of 0.8 U/kg insulin administration. All mice were maintained in individual cages. It was used ACCU-CHEKAdvantage II - (Roche Mannheim, Germany) for reading the blood glucose levels.

Determination of serum LPS

LPS concentration in serum was determined using a chromogenic assay based on a Limulus amebocyte extract (LAL kit-terminal QCL1000). Samples were collected at the time of euthanasia via cardiac puncture to try to minimize as much as possible the chance of contamination. The test is quantitative for Gram-negative bacterial endotoxin and was carried out according to manufacturer's guidelines. We used 50 μL of samples in duplicates. The kit's sensitivity is 0.1 endotoxin units/mL.

Wester blotting

50 μg of total protein obtained from the large intestine of lean and HFD fed mice, was diluted in sample buffer (Biorad, USA) containing 20 mg/mL of 2-β-mercaptoethanol (Sigma-Aldrich). Proteins were denatured by heating for 5 min at 95°C, and were then separated by electrophoresis on a 10% polyacrylamide gel. The proteins were transferred to a nitrocellulose membrane, and blocked for 1 h with 5% milk dissolved in TBS-Tween, incubated with the primary antibody diluted in TBS-Tween. Next, the membrane was washed with TBS-Tween and incubated for 1 h with the secondary antibody. The molecular mass of protein was determined by comparison with the migration pattern of

Rainbow protein or Dual Color (Biorad Laboratories, CA, USA). The primary antibody used was anti-mouse β-actin (1: 10,000), anti-mouse occludin (1:500). The secondary antibody used was anti-mouse (1:3000).

Lamina propria cells/macrophages isolation

At the end of treatment, animals were sacrificed, and cells from large intestine lamina propria recovered. Briefly, the large intestine was separated at the junction with the cecum, and all remaining connective and fat tissue removed. Isolated intestine was then opened longitudinally, cleaned, cut into 0.4–1 cm pieces and washed with ice-cold 25 mM HEPES in PBS. Tissue fragments were then placed in RPMI (Gibco) medium containing 3% fetal bovine serum, 25 mM HEPES, 5 mM EDTA plus 3.5 mM Dithiothreitol and incubated for 15 min in 37°C with gentle agitation. Tissue fragments were recovered via filtering and vigorously washed thrice with 2 mM EDTA in RPMI, discarding supernatants. Washed fragments were minced then incubated in RPMI supplemented with 0.5% fetal bovine serum, 2 mg/mL Collagenase VIII and 0.5 mg/mL DNAse I for 30–40 min at 37°C with gentle agitation. Cell suspension and tissue fragments were filtered through a 70 μm strainer, and dissociated with the rubber end of a syringe plunger. Resulting cell suspension was centrifuged and further filtered through a 40 μm cell strainer. Finally, live cells were passed through a Percoll gradient (35%/70%), recovered from the interface, washed, counted and incubated with antibodies for flow cytometry as described in the section below.

Flow cytometry

After lamina propria cells isolation from CX3CR1 GFP heterozygous mice, the cell suspension was incubated in 5 μgml−1 anti-CD16/32 (1:200), stained with Live Dead Near IR (ThermoFisher, 1:500), and then surface stained with a fluorochrome conjugated monoclonal antibody to CD45 (Pacific Blue, SF18009F, 1:200), CD11b (PECy7, M1/70,1:300), CD64 (BV711, X54-5/7.1, 1:200), MHCII (PercpCy5.5, M5/114.15.2, 1:200), Tim4 (APC, F31-5G3, 1:200), CD4 (BV510, RM4-5, 1:200), CD86 (BV650, GL-1, 1:400), CD80 (APC, 16-10A1, 1:200), CD206 (PE, C068C2, 1:500). For Phagocytosis assay, pHrodo Red Staphylococcus aureus Bioparticles (ThermoFisher, 100μg mL−1) was used according to the manufacturer's instructions. BODIPY LD 540 (developed by Prof. Christoph Tiele[51] was used for neutral lipid staining according to the manufacturer's instructions. CPT1a primary antibody staining (Proteintech) was detected using the Alexa Fluor 647 anti-rabbit secondary antibody (Life technologies). ROS was measured using CellROX Deep Red Flow cytometry assay Kit according to manufacturer instructions (Invitrogen). Active mitochondria were measured using 50 nM of the the mitochondrial mass staining Mito Tracker Deep Red (ThermoFisher) added in the cells in complete media with FCS for 30 min. Data were acquired by flow cytometry on an LSRII or LSR Fortessa (BD Biosciences) and analyzed with FlowJo v.10.1 (Tree Star).

RNA sequencing

Lamina propria cells were prepared for cell sorting as described above (in the lamina propria cells/macrophages isolation section) and incubated in anti-CD16/32, stained with Live/Dead, and fluorochrome-conjugated antibody to CD45, CD11b, CD64, MHCII. The LPMs from mice were CX3CR1 GFP. FACS-sorted CX3CR1^{hi} MHCII^{hi} LPMs using a BD FACS ARIA III, were prepared for RNA extraction. Total RNA was extracted with the RNAqueous-Micro Total RNA Isolation kit (Thermo Fisher Scientific) and quantified using Qubit 2.0 (Thermo Fisher Scientific), according to the manufacturer's instructions. Libraries were prepared using the TruSeq stranded mRNA kit (Illumina) and sequenced in a HiSeq 3000 (Illumina) by the Deep Sequencing Facility at the Max Planck Institute for Immunobiology and Epigenetics. Sequenced libraries were processed with a pipeline optimized by the Bioinformatics core at the Max Planck Institute for Immunobiology and Epigenetics.[52] Raw mapped reads were processed in R (Lucent Technologies) with DESeq2[50] to determine differentially expressed genes and generate normalized read counts to visualize as heatmaps using Morpheus (Broad Institute). Enrichment analysis based on hypergeometric distribution followed by FDR correction for GO terms were made using ShinyGO 0.76 software.[53]

Single cell barcoding and library preparation

Lamina propria cells were prepared for cell sorting as described above (in the lamina propria cells/macrophages isolation section), and incubated in anti-CD16/32, Live/Dead dye and an anti-CD45 fluorochrome-conjugated antibody and isolated using a BD FACS ARIA III cell sorter. Recovered CD45 positive cells were prepared for scRNAseq analysis using a 10X Genomics Chromium Controller. Single cells were processed with GemCode Single Cell Platform using GemCode Gel Beads, Chip and Library Kits (v2) following the manufacturer's protocol. Libraries were sequenced on HiSeq 3000 (Illumina). Samples were demultiplexed and aligned using Cell Ranger 2.2 (10X Genomics) to genome build GRCh38 to obtain a raw read count matrix of barcodes corresponding to cells and features corresponding to detected genes. Read count matrices were processed, analyzed and visualized in R using Seurat v. 3 and Uniform Manifold Approximation and Projection (UMAP) as a dimensionality reduction approach. Differentially expressed genes, with greater than a 1.2-fold change and an adjusted p value of less than 0.05, were obtained and compared across clusters using the UpSet methodology. Unbiased cell classification was based on scGate[32] annotation to evaluate the strength of signature marker expression in each cell. Gene expression scores were calculated using UCell. The LAM signature was based on Jaitin et al., 2019.[20] The efferocytosis signature was based on a GO term. OXPHOS and Glycolysis are based on KEGG. Heat shock and Ifn signatures were based on an r Package from the Carmona lab in Lausanne (UCell score creators).

Lipidomics

The protocol for lipid extraction was adapted from Matyash et al.[54] Frozen cell pellets (5×10^5 cells) were resuspended in ice-cold PBS and transferred to glass tubes before the addition of methanol and methyl *tert*-butyl ether. The tubes were then shaken for 1 h at 4°C. Water was added to separate the phases before centrifugation at 1000*g* for 10 min. The upper organic phase was collected and dried in a Genevac EZ2 speed vac. Samples were resuspended in 2:1:1 isopropanol: acetonitrile:water prior to analysis. LC-MS was carried out using an Agilent Zorbax Eclipse Plus C18 column using an Agilent 1290 Infinity II UHPLC in line with an Agilent 6495 Triple Quad QQQ-MS. Lipids were identified by fragmentation and retention time, and comparison to standards, and were quantified using Agilent Mass Hunter software. Comparisons were made between relative amounts of lipid between conditions, extracted from equivalent cell numbers. Peak areas were quantile-normalized across the batch to generate the lipid intensities used for the plots and subsequent statistics shown in this manuscript.